Functionality in single-molecule devices: Model calculations and applications of the inelastic electron tunneling signal in molecular junctions

L. K. Dash, H. Ness, M. J. Verstraete, and R. W. Godby

Additional information on J. Chem. Phys.

Functionality in single-molecule devices: Model calculations and applications of the inelastic electron tunneling signal in molecular junctions

L. K. Dash,[1,2,a)] H. Ness,[1,2] M. J. Verstraete,[2,3] and R. W. Godby[1,2]

[1]*Department of Physics, University of York, Heslington, York YO10 5DD, United Kingdom*
[2]*European Theoretical Spectroscopy Facility (ETSF)*
[3]*Institut de Physique, Université de Liège, B-4000 Sart Tilman, Belgium*

We analyze how functionality could be obtained within single-molecule devices by using a combination of non-equilibrium Green's functions and *ab initio* calculations to study the inelastic transport properties of single-molecule junctions. First, we apply a full non-equilibrium Green's function technique to a model system with electron-vibration coupling. We show that the features in the inelastic electron tunneling spectra (IETS) of the molecular junctions are virtually independent of the nature of the molecule-lead contacts. Since the contacts are not easily reproducible from one device to another, this is a very useful property. The IETS signal is much more robust versus modifications at the contacts and hence can be used to build functional nanodevices. Second, we consider a realistic model of a organic conjugated molecule. We use *ab initio* calculations to study how the vibronic properties of the molecule can be controlled by an external electric field which acts as a gate voltage. The control, through the gate voltage, of the vibron frequencies and (more importantly) of the electron-vibron coupling enables the construction of functionality: nonlinear amplification and/or switching is obtained from the IETS signal within a single-molecule device. © *2012 American Institute of Physics*. [http://dx.doi.org/10.1063/1.3684627]

I. INTRODUCTION

Single-molecule electronics has shown significant progress in recent years. Aviram and Ratner first proposed in the 1970s electronic devices where a single molecule functions as the active element.[1] Since then a variety of interesting effects has been observed in the transport properties of single molecules, including rectification, negative differential resistance, and switching. The molecules usually employed are organic conjugated molecules with strongly delocalized π-electrons along the molecular backbones (and eventually functional chemical groups acting as electron donors or acceptors), and are natural candidates for bottom-up assembly of electronic devices. Chemical synthesis is a massively parallel method to create identical molecules by the mole. Their structures and electronic properties can be tailored virtually at will and can be characterized by several spectroscopic and structural probe techniques. Thus they are ideal building blocks for electronic devices.

However, to make even the simplest molecular electronic device—a single molecule connected between two electrodes—presents several practical difficulties. The fabrication of the nanojunction is a challenge because of the difference in scales between the molecule, the electrodes, and the small gap between them. Moreover, it is even more difficult to verify that the intended molecule is indeed in the junction, that it is well connected, and that it is oriented in the expected manner with respect to the electrodes. Several

methods are used to create such nanojunctions (e.g., mechanical break junctions,[2,3] crossed wires,[4] and scanning probe microscopy[5,6]). Each technique has its own advantages. For example, some of them can be cooled to low temperature, others provide a good control of the electrode spacing, or provide images of the contact area. However, the most crucial and as yet uncontrolled point is the nature of the contacts between the molecule and the electrodes. This is pivotal, since the transport properties of nanojunctions do not depend just on the intrinsic properties of the molecules, but also on the nature of the contacts. Although there is an increasing amount of research into the control of these contacts by tailoring the end groups of the molecule anchoring on the surface,[6–8] there is still a great deal of uncertainty about the specific nature of the contacts. These change from device to device, or even fluctuate during a single experiment, because of thermal effects (atom migration at the electrode surface) or of current-induced effects. Hence, it is extremely difficult to produce molecule junctions with reproducible properties.

Other properties of current-carrying molecular junctions are also important to understand, such as the nature and the effects of electron-vibron coupling on the molecule. Such a coupling can modify the transport properties of the junctions at a particular threshold voltage and is also responsible for heating effects in the junctions. Several groups have already performed inelastic electron tunneling spectroscopy (IETS) on molecular junctions to obtain a signature from the vibration modes of the molecules in the nanojunction.[4,9–18]

---

a)Electronic mail: louise.dash@york.ac.uk.

136, 064708-1

The realization of a true single-molecule device, with three terminals, has been achieved recently.[19] The transport properties through the source and drain are directly modulated by an external gate voltage as in a conventional field-effect transistor. However, in the molecular transistor, the gate voltage modifies the molecular orbital energies. In Ref. [19], the authors also studied the effects of the gate voltage and temperature on the IETS signal. They found that depending on the nature of the molecule, the IETS signal is nearly independent of the gate voltage (for a molecule with a σ-saturated alkyl backbone), however significant modifications of the IETS features' intensity and line shape exist for π-conjugated molecules with an aromatic ring. Their results indicate that both conductance and IETS signal can be modified and controlled by a gate voltage.

Full *ab initio* calculations for a realistic single-molecule with three terminals (source, drain, and gate) are extremely computationally demanding, especially for self-consistent calculations and/or calculations for realistic non-equilibrium conditions. Non-equilibrium transport properties have been calculated for realistic systems of single-molecules connected to two terminals by using density-functional theory (DFT).[20–30] Calculations in the presence of a third gate electrode are rare[31–33] and usually use model Hamiltonians (i.e., tight-binding or extended Hückel). In this paper, we address the problem of functionality in three-terminal single-molecule devices by using a combined (two step) theoretical framework. We discuss the use of both the electronic and the vibronic properties of the molecule to achieve a device with functionality.

The first step consists of a detailed analysis of the full non-equilibrium transport properties of a model system. We study the effects of the contacts between the molecule and the source and the drain on the conductance and the IETS signal. The presence of the gate voltage is incorporated in the position of the molecular levels and generates transitions between different transport regimes (resonant and off-resonant). We use a full non-equilibrium Green's function (NEGF) technique.[34,35,37–58] In order to explore a wide range of experimental contact geometries, we first study a model system, in which two parameters (the contact strength and the corresponding fractions of potential drop) (Refs. [40] and [59]) characterize the molecule-lead coupling. We show that the IETS signal is much less sensitive to the nature of the contact than the conductance itself.

The second step consists of applying the principle found in the first step to a more realistic model. We study the influence of an external electric field on the electronic and vibronic properties of a realistic molecular system based an ethynylphenyl-based backbone by using *ab initio* calculations.[60] Having shown, for the model system, that the IETS signal is nearly independent of the nature of contacts, we concentrate on an isolated molecule and extract the relevant physical quantities (vibration frequencies and electron-vibron coupling matrix elements) in the presence of the electric field which simulates the presence of a gate electrode.

Finally, we discuss and show the possibility of using the IETS signal, rather than the current or the conductance, to

form functional nanodevices with switching, nonlinear amplification or sensor functionality by using our *ab initio* calculations for the conjugated molecule.

II. NON-EQUILIBRIUM TRANSPORT AND THE EFFECT OF THE CONTACTS

We use a NEGF technique to calculate self-consistently the full non-equilibrium inelastic properties of a molecular junction. Using a model system to reduce these calculations to a tractable size, we concentrate on a single molecular level coupled to a single vibrational mode. A full description of our methodology is provided in Refs. [34], [37], and [35].

This approach allows us to study how variations at the contacts modify the transport properties of the junction. These include experimentally uncontrollable modifications of the molecule-lead coupling due to the experimental environment—such as thermal fluctuation, diffusion of atoms at the surface of the leads, variation of the gap of the nanojunction, the presence of impurity molecules around the nanojunction, etc. The consequence of these modifications, and the reason they limit the reproducibility of functionalized junctions, is to change the geometry of the contacts, and therefore the strength of electronic coupling between the molecule and the leads, and the corresponding potential drops at the contacts.

In our model, the central region of the nanojunction, i.e., the molecule, is described by a simple electron-vibron coupling Hamiltonian

$$H_C = \varepsilon_0 d^\dagger d + \hbar\omega_0 a^\dagger a + \gamma_0(a^\dagger + a)d^\dagger d, \qquad (1)$$

where one electronic molecular level ε_0 and one vibration mode with energy ω_0 are coupled together via the coupling constant γ_0. The electron and phonon creation/annihilation operators are $d^\dagger/d$ and $a^\dagger/a$, respectively.

The central region is then coupled to two non-interacting Fermi seas each at their own equilibrium, characterized by the left and right Fermi levels μ_L and μ_R, via two hopping matrix elements t_{0L} and t_{0R} which represent the strength of electronic coupling between the molecule and the leads.

All the properties of the nanojunctions (electronic density, spectral functions, current density) are determined from the knowledge of the NEGF of the central region.[34,35,37] For example, the retarded Green's function of the central region is given by

$$G^r(\omega) = \left[\omega - \varepsilon_0 - \Sigma_L^r(\omega) + \Sigma_R^r(\omega) + \Sigma_{e-\text{vib}}^r(\omega) \right]^{-1}, \quad (2)$$

where Σ_α^r is the self-energy arising from the $\alpha = L, R$ lead and $\Sigma_{e-\text{vib}}^r$ is the self-energy arising form the electron-vibron interaction. The latter is calculated from Feynman diagram expansion of the interaction.[34] In this section, we calculate $\Sigma_{e-\text{vib}}$ from the lowest order expansion of the electron-vibron interaction (first Born or Hartree-Fock level of approximation).[34,35] The calculations are performed self-consistently.[34,36]

Within our NEGF model, the electrostatics are not solved self-consistently with the non-equilibrium electron charge density, and we thus have another degree of freedom for the
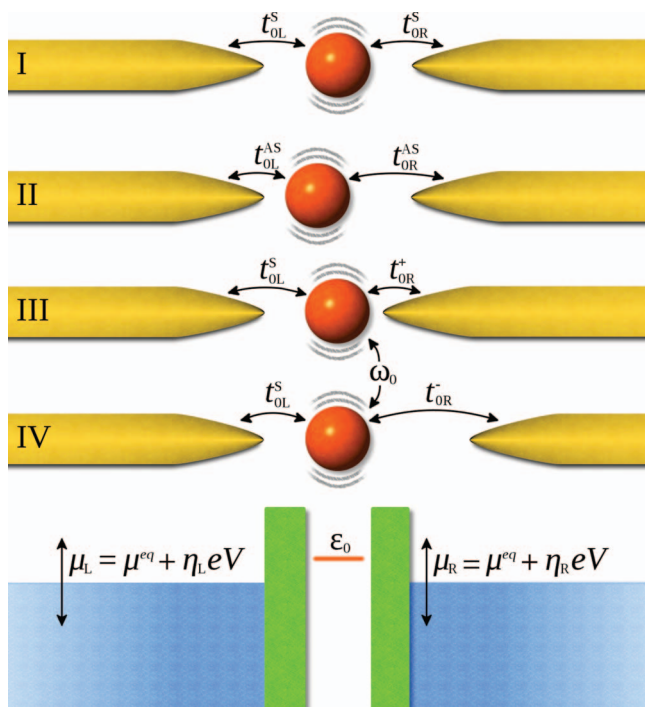
FIG. 1. Schematic representation of our model system. Case (I) shows a symmetric coupling at the contacts, with $t_{0L}^{S} = t_{0R}^{S}$. Cases (II) to (IV) are asymmetric junctions. In Case (II) the total gap is kept constant, but there is a variation in the position of the central region, i.e., $t_{0L}^{AS} + t_{0R}^{AS} = t_{0L}^{S} + t_{0R}^{S}$. In Case (III) the total gap is compressed, $t_{0L}^{AS} + t_{0R}^{AS} < t_{0L}^{S} + t_{0R}^{+}$, while in Case (IV) it is expanded, $t_{0L}^{AS} + t_{0R}^{AS} > t_{0L}^{S} + t_{0R}^{-}$.

potential drops at the contacts. At equilibrium, the whole system has a single and well-defined Fermi level μ^{eq}. Out of equilibrium, a finite bias is applied across the junction, giving Fermi levels $\mu_{L,R} = \mu^{eq} + \eta_{L,R} eV$. Following Ref. 59, the fraction of electrostatic potential drop at the left contact is $\eta_{L} = +\eta_{V}$ and $\eta_{R} = -(1 - \eta_{V})$ at the right contact, with $\eta_{L} - \eta_{R} = eV$ and $\eta_{V} \in [0, 1]$, as shown in Fig. 1.

The parameter η_{V} characterizing the potential drop at the contact is related to the other parameters of the junction, as we can see from the following: Let us consider three typical cases. For the first, when the coupling at the contacts is symmetric, i.e., when $t_{0L} = t_{0R}$, it is reasonable to assume a symmetric potential drop, i.e., $\eta_{V} = 1/2$. In the second case, the coupling is very strong on one side, for example $t_{0L} \gg t_{0R}$, the left Fermi level μ_{L} is pinned to its equilibrium value μ^{eq} and there is a large tunneling barrier at the right contact where all the potential drops occur, i.e., $\mu_{R} = \mu^{eq} + eV$. Finally, we have the opposite case, when $t_{0L} \ll t_{0R}$, the right Fermi level μ_{R} is pinned to μ^{eq} all the potential drops occur at the left contact, i.e., $\mu_{L} = \mu^{eq} + eV$.

For intermediate cases, it is therefore reasonable to assume a lowest order linear dependence of the parameter η_{V} with the hopping integral parameters $t_{0L,R}$, and hence we choose the following relation $\eta_{V} = t_{0R}/(t_{0L} + t_{0R})$. We now have a relation between the strength of electronic coupling between the molecule and the leads and the corresponding fractions of potential drop. In reality the hoping integrals depend exponentially on the distance between atoms and the dependence of the fractions of potential drop on such a dis-

tance obeys a different relation. In principle, the later depends on the dielectric properties of the fully connected molecular junctions. Examples of fractions of potential drop η calculated for realistic molecular junctions, with symmetric and asymmetric coupling, are given in Ref. 61.

In the following, we will consider four different cases, as depicted in Fig. 1, corresponding to different possible modifications of a symmetric nanojunction, and calculate their transport properties. However, in all the four cases, the fractions of potential drop will be close to the symmetric case.

We concentrate on the regime corresponding to tunneling through the HOMO-LUMO gap of an organic molecular junction, where the molecular level is well above (or below) the equilibrium Fermi level μ^{eq}. This is a typical behavior for a semiconducting-like molecule sandwiched between two electrodes when the gate voltage is small.

The calculations for the NEGF model system can be reduced to unitless parameters, i.e. normalized by the hopping integral for the semi-infinite one-dimensional leads. We present the most relevant results of our study for the following set of parameters: $\epsilon_{0} = 1.5$, $\omega_{0} = 0.4$, $\gamma_{0} = 0.35$ and two sets of coupling to the leads: medium coupling with $t_{0L}^{S} = t_{0R}^{S} = 0.27$ and weak coupling with $t_{0L,R}^{S} = 0.15$. A wide range of parameters has been explored, and this choice is the closest to those calculated from first principles (see below).

The fluctuations in the nanojunction introduce variations of the hopping matrix elements shown in Fig. 1: from a symmetric coupling junction, we obtain an asymmetric junction when the position of the molecule inside the gap is varied by a small amount (10%). Hence the left and right hopping integrals are $t_{0L}^{AS} = t_{0L}^{S} + 10\%$ and $t_{0R}^{AS} = t_{0R}^{S} - 10\%$, respectively—case (II). We also consider two cases for which the gap is modified according to $t_{0R}^{+} = t_{0L}^{AS}$ for a compression of the gap—case (III)—and as $t_{0R}^{-} = t_{0R}^{AS}$ for a expansion of the gap—case (IV). The potential drop parameter η_{V} that determines the fractions of potential drop at each contact is calculated from $\eta_{V} = t_{0R}/(t_{0L} + t_{0R})$ as we have explained above. For our set of parameters, we get $\eta_{V} = 0.50$ for case (I), $\eta_{V} = 0.45$ for case (II), $\eta_{V} = 0.5238$ for case (III) and $\eta_{V} = 0.4737$ for case (IV).

The corresponding conductance curves are shown in Fig. 2, and show one main conductance peak for each configuration of the junction as expected. The conductance peak corresponds to a resonant transmission through the main electronic level of the central region, renormalized by the electron-vibron coupling, i.e. a peak at $\approx \tilde{\epsilon}_{0} \sim \epsilon_{0} - \gamma_{0}^{2}/\omega_{0}$. It is clear from Fig. 2 that the bias position of the peak depends strongly on the value of the potential drop factor η_{V} when all the other parameters of the central region are kept unchanged. The width of the peak, proportional to $t_{0L}^{2} + t_{0R}^{2}$, is not greatly affected by the 10% fluctuation of the contacts for the values of the parameters we have chosen.

Results for the IETS signal for the same parameters are shown in Fig. 3, where we clearly observe a rather different behavior in the conductance peaks. Here we see two separate features—the first is a peak at the vibration energy ω_{0}, as we would expect for the off-resonant regime.[35, 37, 40] The amplitude of this feature is proportional to γ_{0}^{2} while the width is
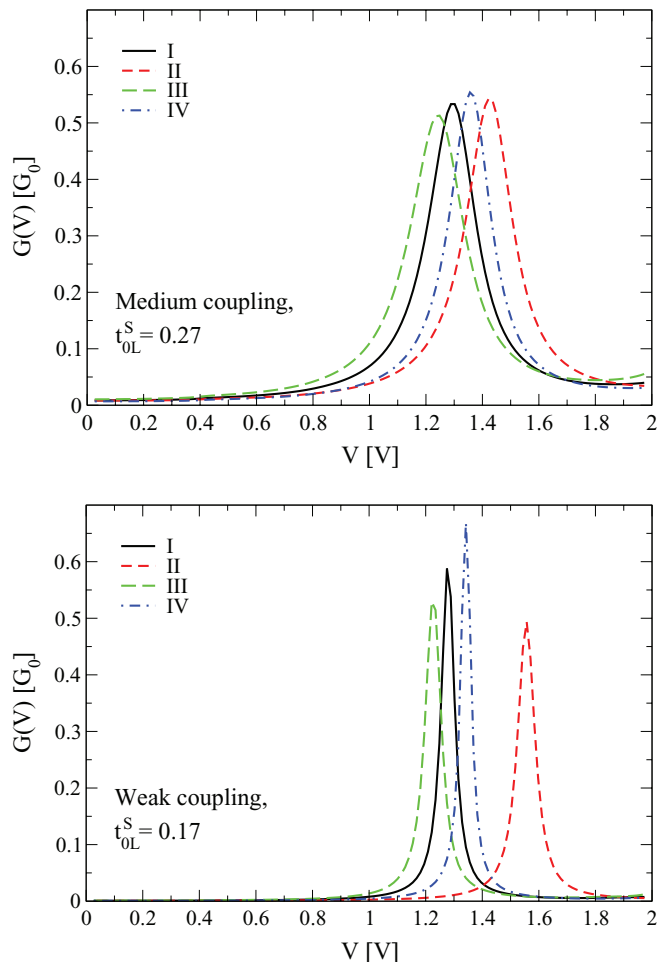
FIG. 2. Dynamical conductance $G(V) = dI/dV$ versus applied bias for the four cases depicted in Fig. 1: symmetric (I) and asymmetric cases (II, III, IV). The top panel shows medium coupling to the leads ($t_{0L}^S = 0.27$) and the bottom panel weak coupling ($t_{0L}^S = 0.17$). Both sets of calculations show that, even for small variations of the potential drop parameter η_V, the position of the main conductance peak is strongly dependent on the fraction of potential drop at the contacts.

dependent on the other parameters of the junctions.[56,62] At higher biases we observe the conductance peak, which occurs at the polaron-shifted electronic level $\tilde{\varepsilon}_0$. Increasing the coupling to the leads yields an effective decrease of the conductance peaks accompanied by an increase in the width, as expected. This leads to better contrast in IETS between the pure inelastic feature at ω_0 and features associated with elastic and inelastic resonant tunneling: the amplitude of the inelastic feature is much less dependent on the coupling to the leads.

It is also clear from Fig. 3 that the position in bias of the IETS features around $V = \omega_0$ does not depend at all on the strength of the coupling to the leads and on the fraction of potential drop at the contacts. In other words, the position of the IETS feature is independent of the nature of the contacts. This is the important result of this paper, as it means that the IETS signal is more stable, in terms of spectroscopic information, than the conductance itself. The IETS signal from the internal vibrational modes of the molecule is not strongly dependent on the way the molecule is connected to the leads.
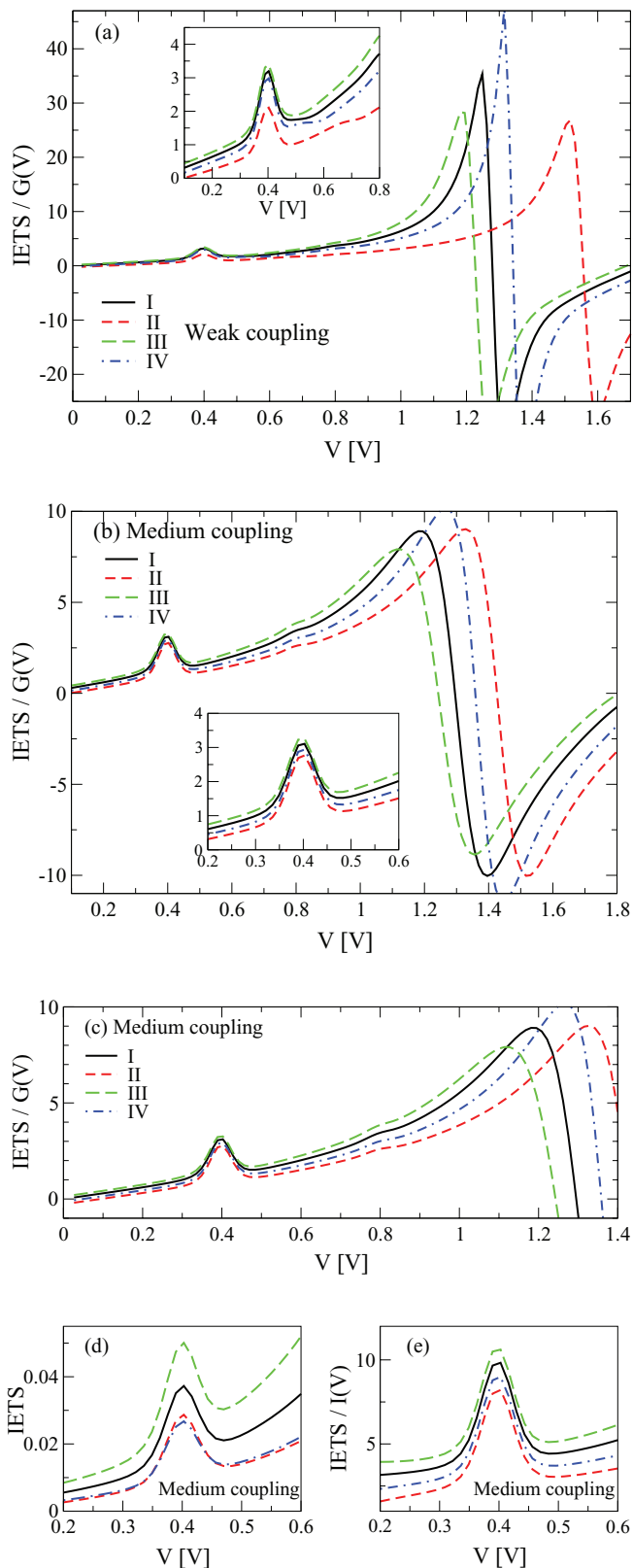

FIG. 3. IETS signal d^2I/dV^2 normalized by the conductance $G(V)$ for the four cases depicted in Fig. 1. The top panel shows data for weak coupling to the leads ($t_{0L}^S = 0.17$), the middle and bottom panels for medium coupling ($t_{0L}^S = 0.17$). Both sets of calculations show that the position of the IETS feature at $V = \omega_0 = 0.4$ is not dependent on the fraction of potential drop at the contacts. The bottom panels show different normalizations of the IETS as well as the bare IETS signal, as different normalization conventions are often used in the experiments. There is no need to show $(d^2I/dV^2)/(I/V)$ since in this bias regime the current is linear $G \sim I/V$.

This occurs because, in spectroscopic terms, the IETS signal depends only on the difference between the left and right Fermi levels. Thus a vibration mode can only be excited by inelastic collision with the charge carriers once the bias exceeds the vibrational energy, i.e. $V \gtrsim \omega_0$, which leads to a corresponding feature in the IETS. Note that this is not dependent on the model of the electron-vibron coupling—it is purely an effect of non-equilibrium inelastic transport at the threshold bias $V \gtrsim \omega_{\text{ext}}$, where ω_{ext} could be any excitation of the system coupled to the injected charge carriers. There are also extreme asymmetric cases for which the line shape of IETS may vary or become a dip rather than a peak,[40] but the position of the feature will nonetheless remain at $V \sim \omega_0$.

The conductance peaks at $V \sim \tilde{\varepsilon}_0$, however, correspond to resonant transmission through electronic levels, with or without vibration replica.[35] Such resonances in the conductance depend on the relative position of the two Fermi levels with respect to the renormalized electronic levels, i.e., similar to band offsets in semiconductors. The conductance peak position is therefore dependent on the fraction of potential drop at the contacts. In our model, the left Fermi level moves up, while the right Fermi level moves down, for positive bias. The fraction of how much μ_L moves up for a given bias is determined by the factor η_V. The smaller η_V, the larger the bias V has to be for μ_L to become resonant with an electronic level $\tilde{\varepsilon}_0$. Such a mechanism explains the variation of the conductance peak positions for the different cases (I–IV) of fluctuations in the junction that we have considered in Fig. 1. These results confirm experimental common knowledge: although an individual molecular device based on the use of the conductance as the key signal may work well,[63] unless the fabrication of the device can be reliably controlled and reproduced then mass production will remain impossible. This is especially true because the exact nature of the lead-molecule contacts is unknown and as yet impossible to reproduce to specification.

The results we have to chosen to present in this section are obtained for a variation of 10% of the hopping integrals. Obviously, larger variations will lead to stronger effects, i.e. more important modification of intensities of both the conductance peaks and the IETS features, and more important shifts of the position of the conductance peak. The IETS features will remain fixed at the same bias. It appears here that even small variations of the hopping integrals lead to substantial effects. As an illustration, let us recall that in reality the hopping integrals between two different electronic orbitals vary exponentially with the distance between the two atoms supporting these orbitals. The zero-point motion associated with quantum fluctuations are of the order of 0.01–0.05 Å, leading to variations in the hopping integrals of a few percent or less. While coordination-induced variations of order of 0.1 Å in the inter-atomic distance (roughly 10% for a carbon double bond, well beyond thermal fluctuations at room temperature) would lead to changes of 20% to 50% (and more) of the hopping integrals. Our choice of 10% variation of the hopping integrals is intermediate between these two regime.

Furthermore, the analysis performed in this section is well suited for large molecular system which have internal vibration modes of atoms not involved in the bonding

of the molecule to the leads. Indeed, for small molecules, most, if not all, of the atoms constituting the molecule are in close contact with the surface of one or both electrodes. In these cases the molecular vibronic properties (frequency of vibration and electron-vibration coupling matrix elements) are strongly dependent on the coupling of the molecule to the lead. All (or most) of the atoms involved in the chemical bonds inside the molecule are also involved in the bonding to the leads. These effects have been clearly shown in experimental as well as theoretical works.[64–67]

However, for larger molecules (molecular wires) it is clear that many vibration modes—the ones mostly located inside the molecular wire—will be much less dependent on the chemistry of bonding of the end atoms of the molecule to the electrodes. These modes are usually the optical-type modes and are strongly coupled to the LUMO and/or HOMO frontier orbitals as we show in Sec. III. It is with these systems in mind that we aim to build functionality. Hence the IETS signal of such systenes rids us of the need to control accurately the nature of the contacts, and is thus a much more useful signal to consider when designing and building functional single-molecule devices. In order to exploit this phenomenon and build a useful device, we need some form of external control over the position and/or amplitude of the IETS feature. This external control could take several forms (magnetic field, chemical concentration, pressure, etc.), but here we propose the use of an external electric field, in a similar way as a gate voltage is used in Ref. 19 to control the conductance.

III. MODIFYING THE ELECTRONIC AND VIBRONIC PROPERTIES OF A MOLECULE WITH A GATE POTENTIAL

We now explore how the properties of the IETS signal we have demonstrated in Sec. II can be used for a more realistic system.

For this we use *ab initio* calculations to study the effect of an uniform electric field, acting as a gate voltage, on the electronic and vibronic properties of a realistic molecular system. We calculate how the corresponding values of ω_0 and γ_0 in our NEGF calculations are modified by the external field for selected vibrational modes coupled to the molecular HOMO and LUMO levels. We then demonstrate in Sec. IV that these results can be used to design a selectively functionalized single-molecule device.

As full *ab initio* calculations for a realistic single-molecule device with three terminals are extremely computationally demanding, especially for self-consistent calculations, and are beyond present computational power if one has to take the full non-equilibrium and many-body effects into account, one has to introduce some approximations.

In the following, as a first step of calculations to analyze the potential of functional devices using the IETS signal, we perform the calculation for an isolated molecule in the presence of an electric field perpendicular to the backbone of the molecule. However, in real devices with metallic electrodes, the electrostatic potential acting on the molecule from an applied field perpendicular to the interelectrode spacing will be substantially distorted, on the scale of the molecule, from an

uniform field we use in the calculations. Hence, the results we show in this section provide only the general trends of the field dependence on the IETS signal for our model *ab initio* calculations.

Furthermore, it is known that in real systems the presence of the electrode and the coupling of the molecule to the electrodes are crucial to determine accurately the charge transfer and transport properties of such a molecular nanojunctions. We have shown in Sec. II that the nature of the contacts (especially the strength of the couplings and the corresponding potential drops) do indeed dominate the properties of the conductance. The contacts also play an important role in other physical transport properties such as heat transport.[68]

However, we have also shown that the IETS signal is virtually independent of these characteristics of the contacts (hence the study of an isolated molecule). Furthermore, we concentrate our calculations on the effects of the electric field on the vibron modes which have a weak amplitudes at the ends of the molecules. Normally, such modes would not be strongly coupled to the electrodes if the molecule were to be fully connected in a realistic molecular device.

As our test system, we choose the molecule 2,5-di [2′-(para-acetylmercaptophenyl)ethynyl]-4-nitro-acetylanilin, shown in Fig. 4(a), which has previously been used for transport measurements in a break junction.[3] Molecules with a similar ethynylphenyl-based backbone but with different redox centers in the middle benzene ring have also been used in self-assembled monolayer transport measurements.[69,70] Another reason to chose this molecule is based on the fact that the IETS signal of conjugated molecules can be modified by a gate voltage has been shown in Ref. 19. Furthermore, our candidate molecule has peripheral chemical groups that provide additional properties.

This molecule has specific properties that we are able to exploit. First, the form of the side-chains provide a permanent electric dipole, so that the component of the electric field (associated with the gate voltage) that is perpendicular to the backbone of the molecule will show substantial effects. In particular, the electric field will polarize the electron cloud along the dipole. In the regime of strong field, the applied electric field might even bend the molecular backbone. Second, we will show that the dominant phonon modes coupling to the HOMO/LUMO levels are situated on the central part of the molecule, and are thus effectively separated from the leads.

Because of this, and the properties of the IETS signal versus the nature of the contacts, we do not include leads in our *ab initio* calculations. Rather, we replace the end groups of the molecule by hydrogen atoms, and then fix these terminal atoms within our supercell when structural relaxations are performed.

We calculate the ground-state electronic and vibronic properties of the system using the ABINIT package.[60] The calculations are performed with Trouiller-Martin pseudopotentials, using the local-density approximation and the exchange-correlation functional from Goedecker *et al.*[71] We use a supercell of size $50 \times 30 \times 50$ [bohr^3] with a plane-wave cutoff of 30 Ry at the Γ-point. The geometries of the molecule in the absence and in the presence of the electrical field are fully relaxed until the maximum force on each atom is less than
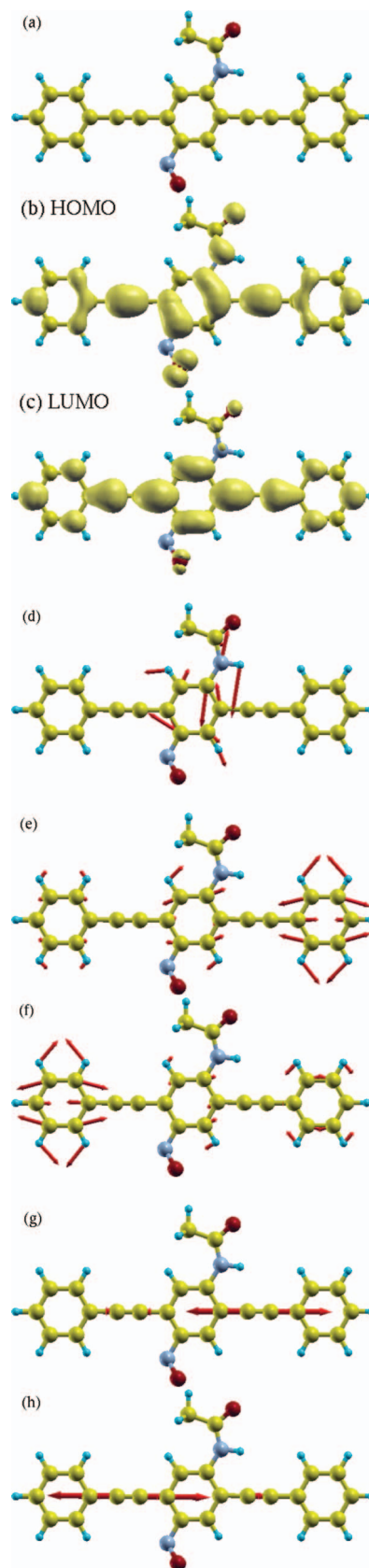

FIG. 4. Molecular wire: (a) ball and stick representation. (b) HOMO state. (c) LUMO state. (d–h) Eigenmodes of vibration. (d) Mode strongly coupled to the HOMO, mode $\lambda = 111$ with $\omega_\lambda \sim 197$ meV; (e–f) Modes strongly coupled to the LUMO, mode (e) $\lambda = 114$ with $\omega_\lambda \sim 206$ meV, and mode (f) $\lambda = 115$ with $\omega_\lambda \sim 207$ meV; (g, h) Modes strongly coupled to both the HOMO and LUMO, mode (g) $\lambda = 118$ with $\omega_\lambda \sim 281$ meV, and mode (h) $\lambda = 119$ with $\omega_\lambda \sim 284$ meV.

0.04 eV/Å. These are sufficient for our analysis of the frequency variation induced by the external field.

We first calculate the molecular structure without any applied field. The relaxed geometry is planar in the (x, y) plane. The molecule has a DFT HOMO-LUMO gap of 2.29 eV and presents a permanent dipole moment $\vec{d} = d_0(x, y, 0)$, lying in the plane of the aromatic cycles, of magnitude $d_0 = 1.878$ D and direction $(x, y) = (\frac{1}{2}, \frac{\sqrt{3}}{2})$ where the x-axis is long the molecular backbone.

The vibronic properties of the molecule are calculated from the dynamical matrix calculated in linear-response DFT (as in Ref. 72):

$$D_{\alpha\beta}^{ij} = \frac{1}{\sqrt{M_i M_j}} \frac{\partial^2 E_{\text{tot}}}{\partial r_{i\alpha} \partial r_{j\beta}}, \qquad (3)$$

where $r_{i\alpha}$ is the displacement of atom i (of mass M_i) α is the reduced direction and E_{tot} is the total energy obtained from the DFT calculation.

The eigenvalues of the dynamical matrix $D_{\alpha\beta}^{ij}$ give the square of the vibron frequencies ω_λ^2 while the eigenvectors are the eigenmodes of vibration $V_{i\alpha}^\lambda$. The electron-vibration coupling matrix elements are calculated as

$$\gamma_{kk'}^\lambda = \sum_{i,\alpha} \langle \phi_k | \sqrt{\frac{\hbar^2}{2\omega_\lambda}} \frac{\partial H}{\partial r_{i\alpha}} | \phi_{k'} \rangle V_{i\alpha}^\lambda, \qquad (4)$$

where H is Hamiltonian of the molecule with atomic positions $r_{i\alpha}$ and $|\phi_k\rangle$ are the corresponding eigenstates.

A ball and stick representation of the relaxed molecule, the corresponding HOMO and LUMO states, and the most relevant vibrational modes are shown in Fig. 4. The corresponding electron-vibration coupling matrix elements γ_{kk}^λ for the $k \equiv$ HOMO, LUMO states are shown in Fig. 5. Clearly

only a few of the vibron modes couple strongly to the HOMO or LUMO states.

It should also be noted that, at the lowest order in the electron-vibron coupling, the amplitude of the IETS features is proportional to $(\gamma_{kk}^\lambda)^2$ as shown in Refs. 47, 62, and 73–76. Therefore, the graphs in Fig. 5 mimic the IETS spectrum in the range of applied bias $V = 0$ to $V = 0.35$ [V]. In that range, one would only see two main peaks around $V = 0.20$ and $V = 0.28$ [V]. Such a behavior justifies *a posteriori* our NEGF analysis in terms of single-mode excitation.

A central question is how the vibronic properties of the molecule (ω_λ for selected modes and γ_{kk}^λ for the same modes and for $k \equiv$ HOMO, LUMO) can be tuned. In our case the vibrations will be modified by applying an external field $\vec{E}$ to the junction. The external field $\vec{E}$ acts as a potential gate which may control the properties of the current flow through the molecule.[19]

Calculations of the electronic ground state and of the vibronic properties of the molecule are performed in the presence of the external electric field using the ABINIT package.[60] Finite electric-field calculations, within periodic boundary conditions, are performed by introducing an appropriate extra Berry phase in the wavefunctions.[77–79]

In the present calculations, we take the electric field to be lying in the plane of the aromatic cycles and to be perpendicular to the main axis x of the molecule, i.e. $\vec{E} = E_0(0, 1, 0)$. In the full three-terminal device, $\vec{E}$ represents the projection of the three-dimensional electric field with the plane of the molecule and perpendicular to its backbone. This is the component that is expected to have the most efficient interaction with the dipole of the molecule. We chose that the magnitude of the field E_0 ranges from 0.001 to 0.020 a.u., i.e., from 0.051 up to 1.025 V/Å. This values correspond to typical values of the electric field between a tip and a sample within a scanning probe microscope setup.[80]

Figure 6 shows how the vibron energy and matrix coupling element vary, for selected vibron modes, as the external electric field is increased. We consider the vibron modes which are the most strongly coupled to the frontier orbitals (Fig. 5). We see that the coupling constant γ_{kk}^λ decreases monotonically for modes $\lambda = 111$ and 119 over a range of $\Delta E_0 = 0.3$ [V/Å] when $E_0 \geq 0.1$ [V/Å], with an overall decrease of 70% for mode 111, and 80% for mode 119. Meanwhile mode 118 decreases much faster, showing a switching-like behavior over a smaller range $\Delta E_0 = 0.15$ [V/Å] with an overall reduction of γ_{kk}^λ larger than 90%. We also see that the applied external field lifts the degeneracy between modes 118 and 119.

In Fig. 7, we represent how the HOMO and molecular level varies with the applied electric field. We see that for the values of the field we use, the variations of the HOMO and HOMO-1 levels are only of a few percent. Assuming that in a three-terminal device, the Fermi level at equilibrium is pined at the mid-gap of the molecule, the gate voltage is modifying the position of the HOMO level but does not induce a transition between the off-resonant transport regime to the resonant transport regime, i.e., the HOMO level is always well below the Fermi level.
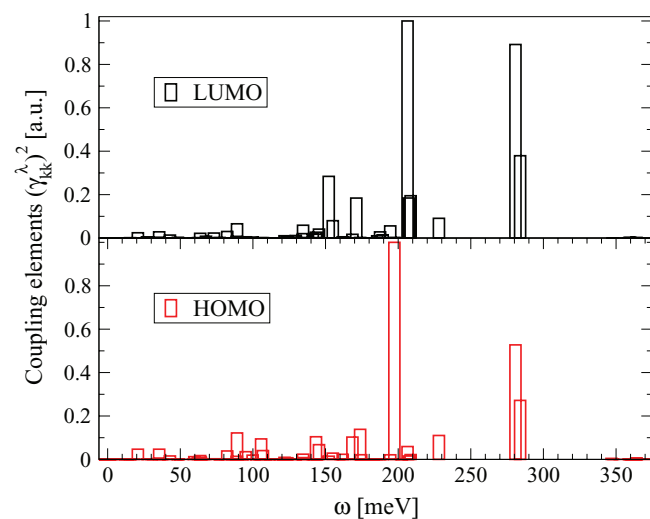

FIG. 5. Electron-vibration coupling: diagonal matrix elements γ_{kk}^λ versus the vibration energy ω_λ for the two HOMO and LUMO Kohn-Sham states k. The amplitude of the matrix elements are normalized to arbitrary units, i.e., $\max(\gamma_{kk}^\lambda)^2 = 1$. Note that since the IETS signal amplitude around $V = \omega_\lambda$ is proportional to $(\gamma^\lambda)^2$, the graphs mimic the IETS signal in the low-bias region. One would get only two significant peaks in the range of applied bias $V = 0$ to $V = 0.35$ [V].
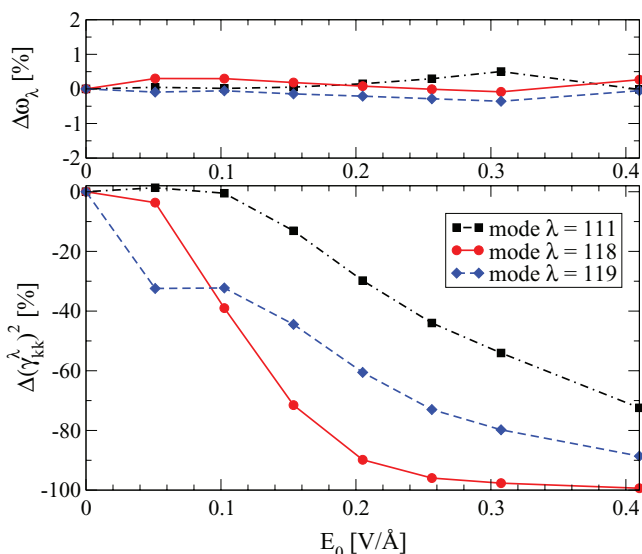
FIG. 6. Relative evolution of the vibron energy ω_λ and coupling matrix elements γ_{kk}^λ to the HOMO state as a function of the external electric field, for modes $\lambda = 111$, $\lambda = 118$, and $\lambda = 119$. The zero-field values for the vibron energies and coupling constants (in meV) are $\omega_\lambda = 197.39$ and $\gamma_{kk}^\lambda = 54.14$ ($\lambda = 111$); $\omega_\lambda = 280.74$ and $\gamma_{kk}^\lambda = 39.32$ ($\lambda = 118$); $\omega_\lambda = 283.93$ and $\gamma_{kk}^\lambda = 28.23$ ($\lambda = 119$), respectively.

IV. APPLICATION TO FUNCTIONALITY IN SINGLE-MOLECULE DEVICES

We now concentrate on the feasibility of obtaining a functional single-molecule device by using the IETS signal. The results of the DFT *ab initio* calculations given in
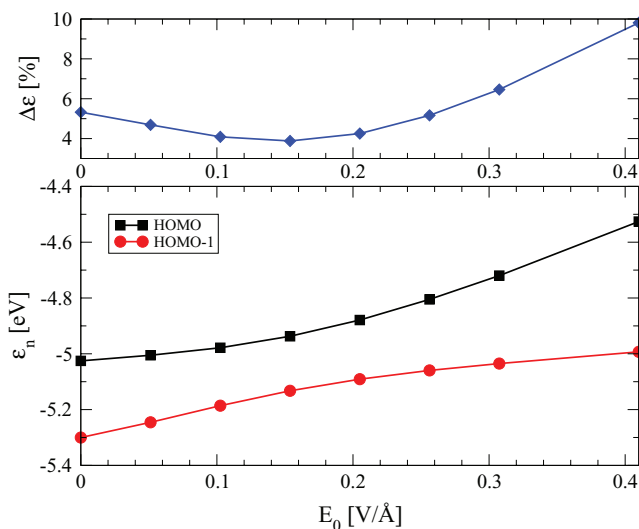

FIG. 7. Relative evolution of the HOMO and HOMO-1 electronic levels ϵ_n versus the applied external field. The zero field value of the HOMO level is $\epsilon_{HOMO} = -0.18468$ Ha $= -5.0254$ eV and $\epsilon_{HOMO-1} = -0.19478$ Ha $= -5.3002$ eV. The top panel shows the relative energy separation between the HOMO and HOMO-1 levels $\Delta\varepsilon = (\varepsilon_{HOMO} - \varepsilon_{HOMO-1})/\bar{\epsilon}$ with $\bar{\epsilon} = |\varepsilon_{HOMO} + \varepsilon_{HOMO-1}|/2$. Two linear regimes or a linear and weak quadratic regime are obtained for the dependence of ϵ_{HOMO} on the external field. The HOMO level varies only by a few percent. The applied electric field would not induce a transition from the off-resonant to the resonant transport regime. Furthermore the energy separation with the HOMO and HOMO-1 levels increases with the applied field, validating even more the single-level analysis used in our model calculations.
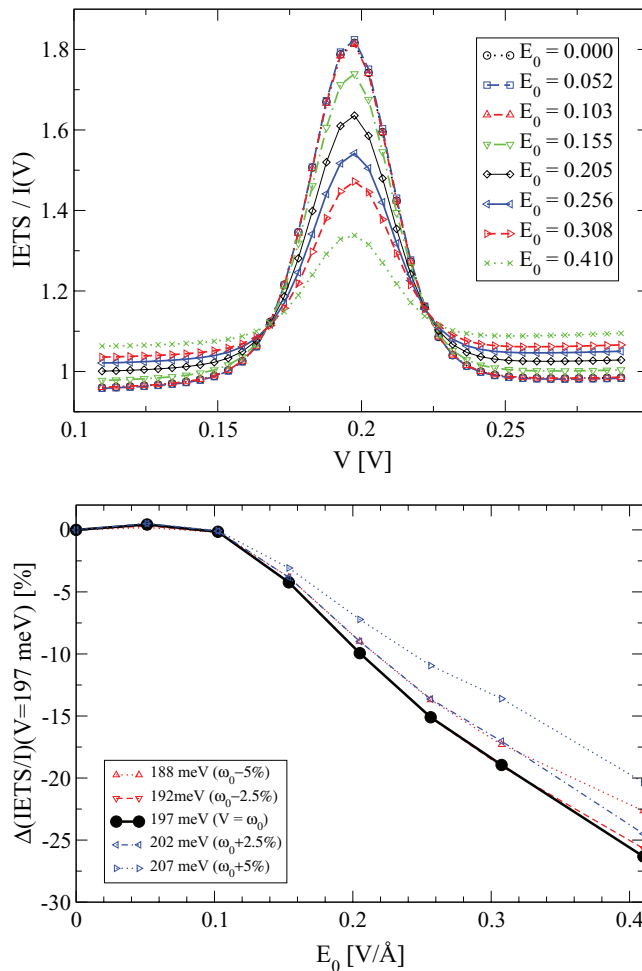

FIG. 8. Top panel: Evolution of the normalized IETS signal around $\omega_\lambda = 197$ meV for mode $\lambda = 111$ for the different values of external electric field E_0 [V/Å]. The IETS signal is normalized by the value of the current $I(V)$ taken at the same bias. The inelastic peak is centered on $\omega_\lambda = 197$ meV for all electric field values, only the peak amplitude and background changes. Bottom panel: Relative evolution of the normalized IETS signal at the inelastic resonance $V = \omega_\lambda = 197$ meV versus the values of external electric field E_0. The evolution of the signal versus the gate voltage (related to E_0) is typical of a nonlinear amplification process when E_0 decreases from a finite value to zero.

Sec. III will be used as input parameters in our NEGF model. The vibron frequency is $\omega_0 \leftarrow \omega_\lambda$, and the electron-vibron coupling constant $\gamma_0^2 \leftarrow (\gamma_{kk}^\lambda)^2$. We take the molecular electronic level ε_0 to be mid-gap, i.e., $\pm(\varepsilon_{LUMO} - \varepsilon_{HOMO})/2$, which is $\sim \pm 1.15$ eV. Finally, we introduce an effective broadening $t_{0L,R}$ of the molecular levels corresponding to the coupling with the leads. The coupling is chosen such that the molecular level broadening is less than the spacing between levels $(\varepsilon_{HOMO} - \varepsilon_{HOMO-1})/3.3 \sim 80$ meV.

Using these values, we calculate the IETS signal around $V \sim \omega_0$, and study how this signal is modified by the external applied field $\vec{E} = E_0(0, 1, 0)$. The upper panels of Figs. 8 and 9 show the evolution of the IETS signal for NEGF calculations with the parameters for mode 111 and mode 118. Here we have chosen to normalize the IETS by the current itself, as it reduces the effect of the slope background on the IETS peaks (see Fig. 3).
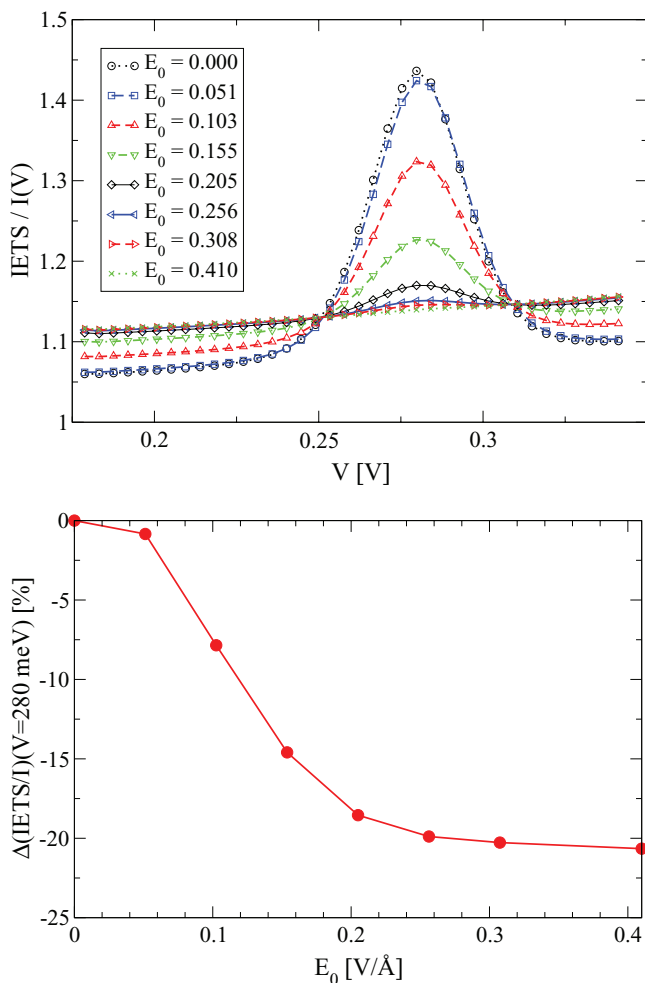
FIG. 9. Top panel: Evolution of the normalized IETS signal around $\omega_\lambda = 280$ meV for mode $\lambda = 118$ for the different values of external electric field E_0. Bottom panel: Relative evolution of the normalized IETS signal at $V = \omega_\lambda = 280$ meV versus the values of external electric field E_0. The evolution of the signal versus the gate voltage (related to E_0) is typical of a strong switching process from high to low values when E_0 increases from 0.05 to 0.20 [V/Å].

The lower panels of Figs. 8 and 9 show the relative evolution of the normalized IETS signal for a fixed source-drain applied bias versus the external electric field acting as a gate voltage. These results demonstrate that we can indeed achieve a functional behavior from the IETS signal when working at low applied bias around the frequencies of the vibron modes (here modes 111 and 118) that are strongly coupled to the HOMO molecular level.

The behavior of the IETS signal in Fig. 8 is typical of a nonlinear amplification of the source-drain current versus the gate voltage represented by E_0. The signal is amplified in a nonlinear manner when E_0 decreases from a finite value to zero. Note that the curve is simply convex with no inflection point.

In Fig. 9 we obtain a typical switching behavior of the IETS signal from two plateaux of high and low value as E_0 increases. Note that now the curve presents an inflection point around $E_0 = 0.10$ [V/Å]; and that the switching occurs over a small range of applied field $\Delta E_0 = 0.15$ [V/Å].

The relative variations of the current-normalized IETS signal is of the order of 20%–25% and is not as important as the relative variation of the corresponding coupling matrix elements $(\gamma_{kk}^\lambda)^2$ shown in Fig. 6. This is to be expected, since the full non-equilibrium inelastic transport properties are not simply related in a linear way to the square of the coupling matrix elements $(\gamma_{kk}^\lambda)^2$, as would be obtained from perturbation theory.[81] In a full non-equilibrium calculation, complex non-linear effects enter into account[40, 57] and cannot be described perturbatively.

In terms of practical devices, the IETS signal could be measured by using an electronic circuit similar to that developed for nonlinear amplification through single fullerene molecules.[82] However, in order to extract the IETS, one would use a lock-in technique for the input source-drain bias, and measure the second harmonic of output voltage at the load resistance.[9] One then gets a signal proportional to the IETS signal since the device works within the linear regime for the source-drain current versus source-drain bias for low applied bias around the vibron frequencies (100–350 meV).

Until now, IETS measurements in molecular nanojunctions have been performed at low temperature.[4, 10–14, 16–18] This is necessary in order to have good mechanical stability of the molecular junctions, as well as a good resolution of the IETS feature which depends on the thermal fluctuations of the soft acoustic-like vibration modes.[83] The width of the IETS features increases with increasing temperature, with a loss of resolution above liquid nitrogen temperature.[12, 19] All this limits the use of the single-molecule devices to temperatures below ~70 K. It can be expected that by working with other candidates of molecular connectors, or by using different concepts to build three-terminal devices (i.e., for example by using carbon-based electrodes[84]), this temperature limit could be lifted.

V. DISCUSSION

Using a two-step theoretical framework we have shown that the IETS signal through molecular junctions can be used to achieve functionality within a single-molecule device. By using a NEGF approach for a model system, we have shown that the IETS is virtually independent of the nature of the contact between the molecule and the source and drain. The electronic and vibronic properties of a realistic molecular candidate (with an ethynylphenyl-based backbone) are calculated using an *ab initio* method. We have shown how an externally applied electric field, simulating the presence of a gate electrode, can control the vibron properties of the molecule and therefore the corresponding IETS signal.

Multi-functionality is demonstrated within a *single* molecule: nonlinear amplification and switching are both present for different vibron modes in the molecular system we have studied. Such functionality should be reproducible from device to device, since the IETS is virtually independent of variations in the molecule-lead contacts.

Furthermore, a recent theoretical study on the difficulty of gate control in molecular transistors[85] has shown that when the molecular energy levels are away from the Fermi level (i.e., the off-resonant transport regime), they can be shifted by

the gate voltage. However, when the molecular levels move close to the Fermi level, the shifts become extremely small and almost independent of the gate voltage. This indicates that it may be difficult to use the gate voltage to control transition in the conductance between the off-resonant regime ("OFF" state) and the resonant regime ("ON" state). This difficulty does not occur in our scheme, since we do not rely on the use of the conductance as the functional signal.

In the present study we have considered the low electric-field regime for the control of the IETS at finite bias. In this regime, most of the functionality comes from the dependence of the coupling matrix elements γ_{kk}^{λ} on the electric field, while the vibron frequencies are more or less constant. In the regime of stronger electric field, the polarization of the electronic clouds may be strong enough to lead to modification of some chemical bonds in the molecule. We expect then that the variation of the vibron frequencies will be important and the displacement of the vibron frequencies will dominate the functionality of the single-molecule device.

We can now suggest designing single-molecule sensors in the following manner: one uses a molecule with peripheral chemical groups that can actively react with surrounding molecules. After chemical reaction, the vibron modes of the molecular backbone that couple strongly to the HOMO-LUMO molecular states, and/or the corresponding coupling matrix elements, are modified. One can then monitor the state of the molecular sensor by measuring the evolution of the IETS signal. Finally, the mechanisms we describe above are most relevant in the vibrational theory of the sense of smell (olfaction).[86–88]

[1] A. Aviram and M. Ratner, Chem. Phys. Lett. **29**, 277 (1974).
[2] M. Reed, C. Zhou, C. Muller, T. Burgin, and J. Tour, Science **278**, 252 (1997).
[3] J. Reichert, H. B. Weber, M. Mayor, and H. V. Löhneysen, Appl. Phys. Lett. **82**, 4137 (2003).
[4] J. G. Kushmerick, J. Lazorcik, C. H. Patterson, and R. Shashidhar, Nano Lett. **4**, 639 (2004).
[5] X. D. Cui, A. Primak, X. Zarate, J. Tomfohr, O. F. Sankey, A. L. Moore, T. A. Moore, D. Gust, G. Harris, and S. M. Lindsay, Science **294**, 571 (2001).
[6] L. Venkataraman, J. E. Klare, I. W. Tam, C. Nuckolls, M. S. Hybertsen, and M. L. Steigerwald, Nano Lett. **6**, 458 (2006).
[7] K. Baheti, P. D. Jonathan, A. Malen, P. R. S.-Y. Jang, T. D. Tilley, A. Majumdar, and R. A. Segalman, Nano Lett. **8**, 715 (2008).
[8] M. Dell'Angela, G. Kladnik, A. Cossaro, A. Verdini, M. Kamenetska, I. Tamblyn, S. Y. Quek, J. B. Neaton, D. Cvetko, A. Morgante, and L. Venkataraman, Nano Lett. **10**, 2470 (2010).
[9] K. W. Hipps and U. Mazur, J. Phys. Chem. **97**, 7803 (1993).
[10] N. Liu, N. A. Pradhan, and W. Ho, J. Chem. Phys. **120**, 11371 (2004).
[11] L. H. Yu, Z. K. Keane, J. W. Ciszek, L. Cheng, M. P. Stewart, J. M. Tour, and D. Natelson, Phys. Rev. Lett. **93**, 266802 (2004).
[12] W. Wang, T. Lee, I. Kretzschmar, and M. A. Reed, Nano Lett. **4**, 643 (2004).
[13] L. H. Yu, C. D. Zangmeister, and J. G. Kushmerick, Nano Lett. **6**, 2515 (2006).
[14] D.-H. Chae, J. F. Berry, S. Jung, F. A. C. C. A. Murillo, and Z. Yao, Nano Lett. **6**, 165 (2006).
[15] A. Troisi and M. A. Ratner, Small **2**, 172 (2006).
[16] J. M. Beebe, H. J. Moore, T. R. Lee, and J. G. Kushmerick, Nano Lett. **7**, 1364 (2007).
[17] N. Okabayashi, Y. Konda, and T. Komeda, Phys. Rev. Lett. **100**, 217801 (2008).
[18] Y. Kim, H. Song, F. Strigl, H.-F. Pernau, T. Lee, and E. Scheer, Phys. Rev. Lett. **106**, 196804 (2011).
[19] H. Song, Y. Kim, Y. H. Jang, H. Jeong, M. A. Reed, and T. Lee, Nature (London) **462**, 1039 (2009).
[20] K. Hirose and M. Tsukada, Phys. Rev. Lett. **73**, 150 (1994).
[21] M. Di Ventra, S. Pantelides, and N. Lang, Phys. Rev. Lett. **84**, 979 (2000).
[22] J. Taylor, H. Guo, and J. Wang, Phys. Rev. B **63**, 121104 (2001).
[23] M. Nardelli, J.-L. Fattebert, and J. Bernholc, Phys. Rev. B **64**, 245423 (2001).
[24] M. Brandbyge, J.-L. Mozos, P. Ordejón, J. Taylor, and K. Stokbro, Phys. Rev. B **65**, 165401 (2002).
[25] R. Gutierrez, G. Fagas, G. Cuniberti, F. Grossmann, R. Schmidt, and K. Richter, Phys. Rev. B **65**, 113410 (2002).
[26] T. Frauenheim, G. Seifert, M. Elstner, T. Niehaus, C. Köhler, M. Amkreutz, M. Sternberg, Z. Hajnal, A. D. Carlo, and S. Suhai, J. Phys.: Condens. Matter **14**, 3015 (2002).
[27] Y. Xue and M. Ratner, Phys. Rev. B **68**, 115406 (2003).
[28] E. Louis, J. A. Vergés, J. J. Palacios, A. J. Pérez-Jiménez, and E. SanFabián, Phys. Rev. B **67**, 155321 (2003).
[29] K. Thygesen, M. Bollinger, and K. Jacobsen, Phys. Rev. B **67**, 115404 (2003).
[30] V. García-Suárez, A. Rocha, S. Bailey, C. Lambert, S. Sanvito, and J. Ferrer, Phys. Rev. B **72**, 045437 (2005).
[31] A. W. Ghosh, T. Rakshit, and S. Datta, Nano Lett. **4**, 565 (2004).
[32] F. Zahid, M. Paulsson, E. Polizzi, A. W. Ghosh, L. Siddiqui, and S. Datta, J. Chem. Phys. **123**, 064707 (2005).
[33] S. Vasudevan, K. Walczak, and A. W. Ghosh, Phys. Rev. B **82**, 085324 (2010).
[34] L. K. Dash, H. Ness, and R. W. Godby, J. Chem. Phys. **132**, 104113 (2010).
[35] L. K. Dash, H. Ness, and R. W. Godby, Phys. Rev. B **84**, 085433 (2011).
[36] J. T. Lü and J.-S. Wang, Phys. Rev. B **76**, 165418 (2007).
[37] H. Ness, L. Dash, and R. W. Godby, Phys. Rev. B **82**, 085426 (2010).
[38] T. Mii, S. Tikhodeev, and H. Ueba, Phys. Rev. B **68**, 205406 (2003).
[39] T. Frederiksen, M. Brandbyge, N. Lorente, and A. P. Jauho, Phys. Rev. Lett. **93**, 256601 (2004).
[40] M. Galperin, M. A. Ratner, and A. Nitzan, J. Chem. Phys. **121**, 11965 (2004).
[41] A. Pecchia and A. di Carlo, Rep. Prog. Phys. **67**, 1497 (2004).
[42] D. A. Ryndyk, M. Hartung, and G. Cuniberti, Phys. Rev. B **73**, 45420 (2006).
[43] N. Sergueev, D. Roubtsov, and H. Guo, Phys. Rev. Lett. **95**, 146803 (2005).
[44] J. K. Viljas, J. C. Cuevas, F. Pauly, and M. Häfner, Phys. Rev. B **72**, 245415 (2005).
[45] T. Yamamoto, K. Watanabe, and S. Watanabe, Phys. Rev. Lett. **95**, 65501 (2005).
[46] A. Cresti, G. Grosso, and G. P. Parravicini, J. Phys.: Condens. Matter **18**, 10059 (2006).
[47] M. Kula, J. Jiang, and Y. Luo, Nano Lett. **6**, 1693 (2006).
[48] L. de la Vega, A. Martín-Rodero, N. Agraït, and A. Levy-Yeyati, Phys. Rev. B **73**, 75428 (2006).
[49] A. Troisi and M. A. Ratner, Nano Lett. **6**, 1784 (2006).
[50] M. Galperin, M. A. Ratner, and A. Nitzan, J. Phys.: Condens. Matter **19**, 103201 (2007).
[51] D. A. Ryndyk and G. Cuniberti, Phys. Rev. B **76**, 155430 (2007).
[52] B. B. Schmidt, M. H. Hettler, and G. Schön, Phys. Rev. B **75**, 115125 (2007).
[53] A. Troisi, J. M. Beebe, L. B. Picraux, R. D. van Zee, D. R. Stewart, M. A. Ratner, and J. G. Kushmerick, Proc. Natl. Acad. Sci. U.S.A. **104**, 14255 (2007).
[54] Y. Asai, Phys. Rev. B **78**, 45434 (2008).
[55] C. Benesch, M. Čížek, J. Klimeš, I. Kondov, M. Thoss, and W. Domcke, J. Phys. Chem. C **112**, 9880 (2008).
[56] M. Paulsson, T. Frederiksen, H. Ueba, N. Lorente, and M. Brandbyge, Phys. Rev. Lett. **100**, 226604 (2008).
[57] R. Egger and A. O. Gogolin, Phys. Rev. B **77**, 113405 (2008).
[58] E. J. McEniry, T. Frederiksen, T. N. Todorov, D. Dundas, and A. P. Horsfield, Phys. Rev. B **78**, 35446 (2008).

[59]S. Datta, W. D. Tian, S. H. Hong, R. Reifenberger, J. I. Henderson, and C. P. Kubiak, Phys. Rev. Lett. **79**, 2530. (1997).

[60]X. Gonze, B. Amadon, P.-M. Anglade, J.-M. Beuken, F. Bottin, P. Boulanger, F. Bruneval, D. Caliste, R. Caracas, M. Cote, T. Deutsch, L. Genovese, Ph. Ghosez, M. Giantomassi, S. Goedecker, D. R. Hamann, P. Hermet, F. Jollet, G. Jomard, S. Leroux, M. Mancini, S. Mazevet, M. J. T. Oliveira, G. Onida, Y. Pouillon, T. Rangel, G.-M. Rignanese, D. Sangalli, R. Shaltaf, M. Torrent, M. J. Verstraete, G. Zerah, and J. W. Zwanziger, Comput. Phys. Commun. **180**, 2582 (2009).

[61]J. Chen, T. Markussen, and K. S. Thygesen, Phys. Rev. B **82**, 121412 (2010).

[62]A. Troisi and M. A. Ratner, Phys. Rev. B **72**, 033408 (2005).

[63]S. Y. Quek, M. Kamenetska, M. L. Steigerwald, H. J. Choi, S. G. Louie, M. S. Hybertsen, J. B. Neaton, and L. Venkataraman, Nat. Nanotechnol. **4**, 230 (2009).

[64]J. R. Hahn and W. Ho, Phys. Rev. Lett. **87**, 196102 (2001).

[65]O. Tal, M. Krieger, B. Leerink, and J. M. van Ruitenbeek, Phys. Rev. Lett. **100**, 196804 (2008).

[66]L. Vitali, R. Ohmann, K. Kern, A. Garcia-Lekue, T. Frederiksen, D. Sanchez-Portal, and A. Arnau, Nano Lett. **10**, 657 (2010).

[67]A. Garcia-Lekue, D. Sanchez-Portal, A. Arnau, and T. Frederiksen, Phys. Rev. B **83**, 155417 (2011).

[68]E. C. Cuansing and J.-S. Wang, Phys. Rev. E **82**, 021116 (2010).

[69]J. Chen, M. A. Reed, A. M. Rawlett, and J. M. Tour, Science **286**, 1550 (1999).

[70]J. Chen, Ph.D. dissertation, Yale University, 2000.

[71]S. Goedecker, M. Teter, and J. Hutter, Phys. Rev. B **54**, 1703 (1996).

[72]M. J. Verstraete and X. Gonze, Phys. Rev. B **74**, 153408 (2006).

[73]B. N. J. Persson and A. Baratoff, Phys. Rev. Lett. **59**, 339 (1987).

[74]M. Paulsson, T. Frederiksen, and M. Brandbyge, Phys. Rev. B **72**, 201101 (2005).

[75]Y. C. Chen, M. Zwolak, and M. di Ventra, Nano Lett. **5**, 621 (2005).

[76]J. Jiang, M. Kula, W. Lu, and Y. Luo, Nano Lett. **5**, 1551 (2005).

[77]R. W. Nunes and D. Vanderbilt, Phys. Rev. Lett. **73**, 712 (1994).

[78]R. W. Nunes and X. Gonze, Phys. Rev. B **63**, 155107 (2001).

[79]I. Souza, J. Íñiguez, and D. Vanderbilt, Phys. Rev. Lett. **89**, 117602 (2002).

[80]H. Ness and A. J. Fisher, Phys. Rev. B **55**, 10081 (1997).

[81]Y. C. Chen, M. Zwolak, and M. di Ventra, Nano Lett. **4**, 1709 (2005).

[82]C. Joachim and J. K. Gimzewski, Chem. Phys. Lett. **265**, 353 (1997).

[83]H. Ness, J. Phys.: Condens. Matter **18**, 6307 (2006).

[84]S. Tuukkanen, S. Streiff, P. Chenevier, M. Pinault, H.-J. Jeong, S. Enouz-Vedrenne, C. S. Cojocaru, D. Pribat, and J.-P. Bourgoin, Appl. Phys. Lett. **95**, 113108 (2009).

[85]D. Hou and J. H. Wei, "The difficulty of gate control in molecular transistors," e-print arXiv:1109.5940v1.

[86]L. Turin, J. Theor. Biol. **216**, 367 (2002).

[87]J. Brookes, F. Hartoutsiou, A. Horsfield, and A. M. Stoneham, Phys. Rev. Lett. **98**, 038101 (2007).

[88]M. I. Franco, L. Turin, A. Mershin, and E. M. C. Skoulakis, Proc. Natl. Acad. Sci. U.S.A. **108**, 3797 (2011).